Dynamics of Cosmological Inflation

J C Stephenson

Contents

Abstract

The dynamics of cosmological inflation are usually posed in terms of the simple 'slow roll' model to govern the evolution of the scalar inflaton field. We will focus on a novel numerical study of a more precise but non-trivial dynamics, that of Hamilton-Jacobi (HJ) inflation, evaluate the implications of this more exact dynamics using data from the Planck 2018 report, and conclude the relevance of separatrices (often called attractors) in HJ dynamics. In particular, restrictions on observables r and n_s require a certain adherence of inflationary solutions to separatrices as early as $\gtrsim 60$ e-folds before the end of inflation in the cases we have considered, which is a new result.

Introduction

Cosmology is the study of the Universe on the largest spacial and temporal scales - it concerns the evolution of the Universe, and as a result its origin. The Big Bang theory, founded on the realisation that an expanding universe was once much more compact, is the well known but unsatisfactory 'answer' to the origin of the Universe, and the term inflation refers to an epoch of rapid expansion predicted to occur in the early Universe which produces a more satisfactory theory of the origin of the Universe.
The structure of this report is as follows:

- Sections 1 and 2 present necessary elements of classical cosmology and cosmological inflation (the well-versed reader will need only skim this at most). Section 3 sets up the 'homogeneous background' dynamics we will need in later sections. I hope that these sections form a succinct training for a regular reader of mathematical sciences but a novice in cosmology, introducing for example expanding and non-expanding frames of reference as well as a notion of particle horizon as a measure of satisfying the horizon problem which are generally useful concepts.
- In section 4 we outline the theoretical basis by which small perturbations to the homogeneous model predicts observables on whose values we have good restrictions. This can be represented in terms of only the homogeneous part of the model, but this derivation is well-covered elsewhere and it is not useful for us to repeat this. After this, we describe how to compare so-called 'slow roll' models of inflation with data using the example of so-called 'monomial potentials'
- Section 5 argues for and describes the numerical integration scheme for Hamilton-Jacobi inflation I have designed for this project, including a focus on the necessary elements of the phase portrait, then demonstrates some examples of what one can do with this.
- Section 6 covers the main insights of this project.

Conventions

We will choose some canonical units - the speed of light c and (during non-classical considerations) Planck's constant $\hbar$ are given by the dimensionless constant 1; this choice implicitly changes the units of some quantities from SI so one would need to re-dimensionalise later if we want to interpret quantities in standard units. In the same vein, with $M_{pl} := \frac{1}{\sqrt{8\pi G}}$ (G is Newton's gravitational constant) we choose units such that $M_{pl} = 1$.

1 Cosmology review

1.1 Principle Assumption

The Cosmological Principle - the Universe is spatially isotropic and homogeneous, which is a valid model for large distance scales $\gtrsim$ 100Mpc [16]. More specifically, the assumption is that observables representing (local) physical quantities important to the model in question define constant fields on physical space.

1.2 Frames of reference

The Universe is expanding - the space between bodies is increasing on a large scale. We can set a **comoving frame x**, comoving with respect to expansion, and define $a(t)$, known as the scale factor, in using it to relate $\mathbf{x}$ to the real frame position $\mathbf{r}(t)$;

$$\mathbf{r} = a\mathbf{x}.$$

Notably, the **cosmic time** t is the time measured by clock stationary in the comoving spatial frame[13]. It is advantageous to consider both frames and translate between them - much of the physics is simpler in the real frame as effects of universal expansion are incorporated into the coordinates of $\mathbf{r}$, but space and time are independent in the comoving frame so derivatives will be quoted with respect to this frame. With this advantage of $\mathbf{r}$ in mind, this is an alternative measure of time to be called a **comoving time** which incorporates universal expansion into the time coordinate as opposed to the spatial coordinate, but this will only be used briefly in this essay, so we shall mention it later.

We can scale a and $\mathbf{x}$ by multiplying one by a constant λ an the other by $\frac{1}{\lambda}$, effectively choosing the time at which $a = 1$. We can define the **Hubble parameter** which is independent of such scaling;

$$H(t) = \frac{\dot{a}}{a}.$$

We can assume $H > 0$. As is usual in simple physical models there are unique solutions to the ODE $\frac{\dot{a}}{a} = H(t)$ as we expect a to be quite smooth[1]. If at any time $H = 0$, the so-

[1]The very least one would ask for is continuity, and if the expansion of the Universe is attributed to the presence of a mass-energy field causing finite, locally integrable acceleration $\ddot{a}$ on a large scale then a

lution should be one of constant a, which is famously discounted by Hubble [14] following observations of galactic redshift which poses evidence that H has been > 0 for much of (thus all of in sensible models) our past. Altogether, this justifies our opening statement that the Universe is expanding.

1.3 The Friedmann Equation

Consider the Universe as per the Cosmological principle; isotropy and homogeneity require a metric of the form $\mathrm{d}s^2 = -\mathrm{d}t^2 + \mathrm{d}\mathbf{r} \cdot \mathrm{d}\mathbf{r}$ (in natural units). Moving to comoving spatial spherical coordinates $\mathbf{x} = (r, \theta, \varphi)$ we arrive at the Friedmann–Lemaître–Robertson–Walker(FLRW) metric [16]

$$\mathrm{d}s^2 = -\mathrm{d}t^2 + a^2(t)\frac{\mathrm{d}r^2}{1-kr} + a^2(t)r^2(\mathrm{d}\theta^2 + \sin^2\theta \mathrm{d}\varphi^2)$$

where k is (though k will refer to a different quantity after section 2) called the **spatial curvature**, closely related to the Ricci scalar curvature. From Einstein's field equations, we get the **Friedmann equation**, which we quote as

$$H^2 = \frac{1}{3}\rho - \frac{k}{a^2}. \tag{1}$$

This often appears with a separate constant $\frac{\Lambda}{3}$ added on the right; this can be incorporated into ρ. The evolution of ρ is governed by the equation below, the **fluid equation**. By forming an analogy between the massive medium and a gas, we can assign the homogeneous medium a pressure p:

$$\dot{\rho} + 3H(\rho + p) = 0. \tag{2}$$

The fluid equation is also a result of the continuity equation for the stress-energy-momentum tensor associated with ρ. These equations also give rise to

$$\frac{\ddot{a}}{a} = -\frac{2}{3}(\rho + 3p). \tag{3}$$

A striking feature of the Universe is its curvature, for which $\rho_c = 3H^2$ the critical density is relevant; $\rho = \rho_c \Leftrightarrow k = 0$. Defining

$$\Omega = \frac{\rho}{\rho_c}$$

as the density parameter, we rewrite (1) as

$$\Omega - 1 = \frac{k}{(aH)^2}. \tag{4}$$

is locally C^1.

The shape of the Universe is determined by k, though it and other quantities are often thought of in terms of Ω:

- $\Omega = 1 \Leftrightarrow$ Flat universe, homeomorphic to Euclidean 3-space on a large scale.
- $\Omega < 1 \Leftrightarrow$ Open universe, homeomorphic to hyperbolic 3-space on a large scale.
- $\Omega > 1 \Leftrightarrow$ Closed universe, homeomorphic to the 3-sphere on a large scale.

The famous result of Perlmutter et al[21] is that an open universe is the most likely case, and that $\ddot{a} > 0$ will be the case once the Universe is old enough because the constant Λ is almost certainly > 0.

2 Inflation

2.1 Motivation

Inflation was first proposed so to elaborate on some mysteries in big bang cosmology. Before describing them, we introduce a notion of causal connection.
Events spatially separated by more than the **comoving Hubble radius** $\frac{H^{-1}}{a}$ from an observer will be said to be **causally disconnected** from them. We now justify this; a priori, we do not know exactly how $\dot{a}$ will vary over cosmic time, so although supposedly disconnect/connected points maybe soon enter/leave the neighbourhood of points with which we are said to be causally connected. We thus say that a point in comoving coordinate frame $\mathbf{x}$ is causally disconnected from the origin iff it is moving at a speed in the real frame $a\mathbf{x}$ of greater than or equal to the speed of light, which in our choice of units is 1:

$$\begin{aligned}\mathbf{x}\,\text{is causally disconnected from the origin} &\Leftrightarrow \left|\frac{\mathrm{d}}{\mathrm{d}t}a\mathbf{x}\right| = |\dot{a}\mathbf{x}| \geq c = 1 \\ &\Leftrightarrow \dot{a}|\mathbf{x}| \geq 1.\end{aligned}$$

If an observer is parked at the origin, they are causally connected to a point $\mathbf{x}$ (in the sense described) iff it lies within the **Hubble sphere** in the comoving coordinate frame (the open ball of radius equal to the comoving Hubble radius). In the real frame, the radius of the same Hubble sphere is of course $1/H$.
A more physically exact interpretation is illustrated in figure 1. If H is quite constant over time relative to its magnitude, one could say that the Hubble sphere doesn't change much in the real frame. At the same time, one would say that the Hubble sphere in the comoving frame varies as $1/a$. If a massless particle travels from a point within the Hubble sphere (in whichever frame) in the direction of the origin, it will reach it (constant H assumed), but would not if it started its journey outside the Hubble sphere. In this way, the Hubble sphere outlines the region of potential interaction with the centre.

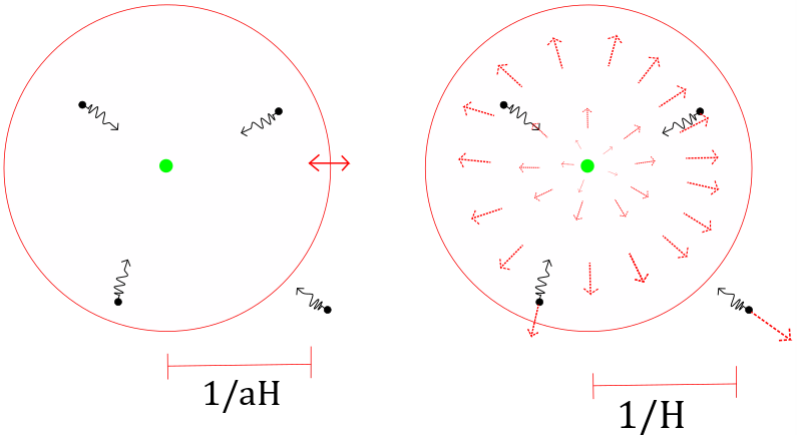

Figure 1: On the right is the picture in the physical/'real' frame **r**; from the observer's perspective, points are receding at a rate in proportion to their length. For relatively constant H the Hubble sphere doesn't change much in this frame of reference. On the left is the same set up but in a comoving frame **x**, from which perspective the Hubble radius varies as $1/aH$.

The remainder of this subsection is based on an exposition by Baumann[7], to whom the reader is referred for details.

The first mystery is dubbed the flatness problem. When one considers a universe whose energy distribution is dominated by either non-relativistic matter or radiation[16] (see figure 3), or a mix of the two, one sees that $\Omega = 1$ is an unstable fixed point; the Hubble radius $\frac{1}{aH}$ increases at least $\propto t^{1/3}$. This finely tunes the value of Ω to very close to 1 at an early cosmic time t. At the least, we can derive from this finding that any extension to the model of cosmology that we have considered so far would ideally predict that Ω was very close to 1 in the early Universe without fine-tuning initial conditions.[2]

Another issue derives from the concern that spatial points in the Universe may have long been causally disconnected, yet observations of the Cosmic Microwave Background (CMB) show that the Universe is fairly homogeneous. Thermodynamically, this is impossible for the model universes we have considered so far.

First, let us define a parametrisation τ of time as far as giving rise to the differential $\mathrm{d}\tau = \frac{\mathrm{d}t}{a(t)}$ where t is the cosmic time; I will call τ a **comoving time**, though often called *conformal time*, because this parametrisation realises the effects of universal expansion if we were to consider a comoving spatial frame.

[2]The reader is encouraged to consider the view of Daniel Baumann [1, 00:20:42] if something like the anthropic principle would discourage them from thinking that this is a mystery at all - retrospectively, analysis of small but significant perturbations on the scale of the observable Universe, as predicted by inflation, make the flatness of the observable Universe seem less likely in big bang cosmology, and there is only so far one can stretch the anthropic principle before one discounts science entirely.

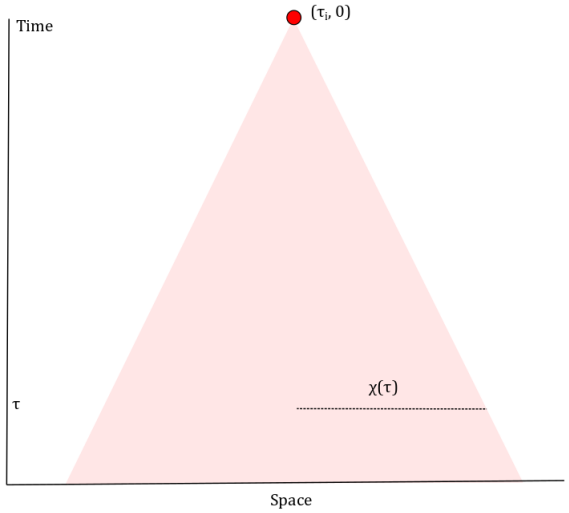

Figure 2: For our sake, the particle horizon of the event $(\tau_i, \mathbf{0})$ refers to $\chi(\tau)$, which is the cross-sectional radius of the backwards light cone, i.e the furthest light could have travelled to reach $(\tau_i, \mathbf{0})$.

	w	$\rho(a)$	$a(t)$	$a(\tau)$
MD	0	a^{-3}	$t^{2/3}$	τ^2
RD	$\frac{1}{3}$	a^{-4}	$t^{1/2}$	τ

Figure 3: Prototype models of a matter dominated (MD) or radiation dominated (RD) universe form can be solved using using the fluid equation and the Friedmann equation. The results are summarised here (table taken from [7]).

τ is also related to the **particle horizon**[3], the greatest spatial separation between the base event and a second event in its backwards light cone, i.e the furthest light can have travelled to arrive at the first event. The particle horizon at time τ for an event at time τ_i is written in comoving coordinates, as

$$\chi(\tau) = \tau_i - \tau = \int_t^{t_i} \frac{\mathrm{d}t}{a(t)}.$$

If we consider a universe dominated by radiation or by matter, we arrive at $\chi(\tau) \propto a(t_1) - a(t)$ or $\chi(\tau) \propto a(t_i)^{\frac{1}{2}} - a(t)^{\frac{1}{2}}$ respectively. Therefore, the model we have built so far predicts that the Universe was just as causally disconnected in the past.

These two problems can be rephrased as the issue that the dynamics of the pressure and density fields in our model define an ill-posed Cauchy problem - we do not have stability with respect to initial conditions.

[3]this often refers to the backwards light cone itself.

2.2 Inflation as a solution to the Horizon and Flatness problems

Cosmological **inflation** is the accelerated expansion of the Universe; inflation is occurring iff $\ddot{a} > 0$. Applying the definition of H and (3) we get two equivalent characterisations of inflation:

$$\begin{aligned} \ddot{a} > 0 &\Leftrightarrow \frac{\mathrm{d}}{\mathrm{d}t}\frac{1}{aH} < 0 \\ &\Leftrightarrow \rho + 3p < 0. \end{aligned}$$

The first condition is exactly that the comoving Hubble radius is a decreasing function of time, i.e the observable Universe grows smaller. We thus have a passing interpretation of inflation as the period of time during which the Universe expands in such a way that the some of it expands outwards and leaves our Hubble sphere.
What is again relevant about this quantity is that $\Omega - 1 \propto \left(\frac{H^{-1}}{a}\right)^2$. This implies that Ω is converging (using this word colloquially) to 1 during inflation, so by the end of inflation, which is still very early in the Universe, Ω is very close to 1. This resolves the flatness problem. Regarding the Horizon problem, a period of roughly exponential, sufficiently rapid inflation leads to the possibility of comoving time taking *negative* values while our observed time would be strictly positive; more inflation makes τ_i more negative, and thus $\chi(\tau) = \tau - \tau_i$ is made much larger, thus causally connecting the Universe. Alternatively, we can see that the decreasing Hubble radius opens a mechanism for the Universe having been more causally connected in the past. It is required constraints on motivational quantities like particle horizon and comoving Hubble radius which one uses to decide 'how much' inflation needs to occur.

3 Inflationary dynamics

For now, we take the Cosmological principle very seriously - we will build a dynamics on a uniform substance with no sense of importance of direction, a uniform scalar field. We will also, mainly because it is a good and useful approximation in compared with observations [17], take spatial curvature $k = 0$.

Let $\phi : \mathbb{R}^+ \to \mathbb{R}$ denote the spatially uniform scalar particle field, so ϕ is a function of t only, named the **inflaton field**; we model the Universe as dominated by this energy form during inflation[4]. We also suppose a potential energy $V(\phi)$ of the field[5]. Using Noether's theorem [7] we arrive at the form of the stress-energy-momentum tensor of ϕ, and thus

[4]The reader interested in particle theory would note that this corresponds to a spin-0 substance.

[5]It is sensible to assume that V is only dependent on time through its dependence on ϕ as we don't see time itself as something which can influence a particle to change its state

expressions for the density and pressure of the fields

$$\rho = \frac{1}{2}\dot{\phi}^2 + V(\phi), \tag{5}$$

$$p = \frac{1}{2}\dot{\phi}^2 - V(\phi). \tag{6}$$

Substituting (5) into (1) gives (with $k = 0$)

$$H^2 = \frac{1}{3}\left(\frac{1}{2}\dot{\phi}^2 + V(\phi)\right). \tag{7}$$

Substituting (5) and (6) into (2) gives the **Klein Gordon eqaution**,

$$\ddot{\phi} + 3H\dot{\phi} + V'(\phi) = 0. \tag{8}$$

Using the formulation of inflation in terms of density and pressure, inflation is occuring iff $\dot{\phi}^2 < V(\phi)$.

It is very challenging to solve the dynamics posed here. Before continuing to consider a numerical study of inflationary models, we define a sensible parametrisation of time during inflation which also quantifies the 'amount' of inflation which occurs, i.e is a parametrisation of the dynamically varying scale factor a during inflation.
By definition of H, $a(t) \propto e^{Ht}$. Useful models of inflation such as Slow Roll (see below and [17]) assume that H is approximately constant, for which reason we see inflation as roughly time-exponential spatial expansion. We define

$$N(t) : = \log\left(\frac{a(t_0)}{a(t)}\right) = \int_t^{t_0} H \mathrm{d}t$$

as the **number of e-folds** until the end of inflation corresponding to comsic time $t < t_0$, the end occurring at time t_0. The number of e-folds which occur during inflation is expected [4] to be[6] $N \gtrsim 60$ in order to solve the horizon problem.

3.1 Slow Roll (SR) inflation

Define

$$\begin{aligned}\varepsilon : = -\frac{\dot{H}}{H^2} &= -\frac{\mathrm{d}\log H}{\mathrm{d}\log a} \\ &= -\frac{\mathrm{d}\log H}{\mathrm{d}N}.\end{aligned}$$

[6] In this case, by similar to or greater than 60, we mean similarity of order ± 0.5.

By looking at $\dot{H} + H^2$ (as in [17]), one can deduce that *inflation is occurring iff* $\varepsilon < 1$. Defining now $\eta := \frac{\dot{\varepsilon}}{\varepsilon H}$, **slow roll** inflation is formally occurring iff $\varepsilon, |\eta| \ll 1$, in which scenario the following hold:

- $\varepsilon \simeq \frac{1}{2}\left(\frac{V'}{V}\right)^2$
- $\eta \simeq \frac{V''}{V}$
- $3H\dot{\phi} + V'(\phi) \simeq 0$
- $H^2 \simeq \frac{1}{3}V(\phi)$
- $N \simeq \frac{1}{2}\int_{\phi_0}^{\phi} \frac{V}{V'}\mathrm{d}\phi$, so if the SR conditions are satisfied for some time during inflation, much of the expansion can occur under these conditions

where these are formal approximations which are true in the limiting case of the SR hypothesis.

3.2 Hamilton-Jacobi (HJ) inflation

Differentiating (7), then using the scalar wave equation, gives

$$2\dot{H} = -\dot{\phi}^2, \quad \varepsilon = \frac{\dot{\phi}^2}{2H^2}. \tag{9}$$

Thus, SR inflation is characterised by particularly small $\dot{\phi}$ relative to H. On the contrary, **Hamilton-Jacobi (HJ) inflation** is valid iff $\dot{\phi} \neq 0$. Assuming $\dot{\phi} \neq 0$, we have $\frac{\dot{H}}{\dot{\phi}} = H'$, denoting $\frac{\mathrm{d}}{\mathrm{d}\phi}$ by $\cdot'$, so

$$\dot{\phi} = -2H'(\phi). \tag{10}$$

Substitute this into (7) to arrive at the **Hamilton-Jacobi equation**

$$(H')^2 - \frac{3}{2}H^2 = -\frac{1}{2}V. \tag{11}$$

In this scenario, as $N = \int_{\phi}^{\phi_0} \frac{H}{\dot{\phi}}\mathrm{d}\phi$,

$$N = \frac{1}{2}\int_{\phi_0}^{\phi} \frac{H}{H'} \quad \mathrm{d}\phi. \tag{12}$$

Additionally, (9) gives

$$\varepsilon = 2\left(\frac{H'}{H}\right), \tag{13}$$

thus

$$N = \frac{1}{2}\int_{\phi_0}^{\phi} \sqrt{\frac{2}{\varepsilon}} \quad \mathrm{d}\phi. \tag{14}$$

Given an initial ϕ value and corresponding H value there exists a unique solution to

(11) (using the Picard–Lindelöf theorem for example), provided the initial values are in the right open set. Considering only real H' means that we need $3H^2 \geq V$, and the hypothesis $\dot{\phi} \neq 0$ gives $H' \neq 0$, thus $3H^2 > V$ for all ϕ. Additionally, as mentioned when we defined H, we need $H > 0$. We will analyse this problem on phase space $\mathfrak{D} := \{(x, y) \in \mathbb{R}^2 : 3y^2 > V(x),\, y > 0\}$ where elements of $\mathfrak{D}$ are to be pairs (ϕ, H) in context.

$\varepsilon < 1$ will characterise inflation. Solutions to the HJ equation in the $\phi - H$ plane which represent trajectories of H during inflation are curves which lie in $\mathfrak{D}$ and are sandwiched between the contours corresponding to $\varepsilon = 1$ and $\varepsilon = 0$, so our effective phase space is

$$\mathfrak{D}_{\text{eff}} := \left\{(x, y) \in \mathbb{R}^2 : 0 < \frac{3y^2 - V(x)}{y^2} < 1,\, y > 0\right\}. \tag{15}$$

One would expect that HJ inflation is a virtually perfect base model; in many senses, with respect to the L^∞ norm for example, restricting to approximations of $\phi(t)$ which have 0 velocity at only finitely many times, we can take as desired we can take as good an approximation as desired. In the name of introducing observables against which we can test our models, we consider an extension to the homogeneous, isotropic case we have considered so far.

4 Linear perturbations to the homogeneous model and associated experimental data

One other problem with standard Big-Bang cosmology is that it doesn't predict the formation of structure well - this can again be solved by inflation [10, pp. 18]. In essence, sufficient inflation will transform inhomogeneities on a small scale to ones on a much larger scale. Still, cosmic microwave background (CMB) observations reveal that the Universe, even as far back as the end of inflation, is homogeneous up to fluctuations or relative magnitude 10^{-5} [7, pp.44]. This justifies modelling an observable $X(t, \mathbf{x})$ as a spatially homogeneous part $\overline{X}(t)$, as in the last section, plus a relatively small perturbation $\delta X(t, \mathbf{x})$. This is a model of **linear perturbations** to the homogeneous background, a model which makes room for a quantum theory of inflation to be appended onto the aforementioned (classical) homogeneous theory, resulting in predictions about the structure of the Universe and thus a framework to experimentally test both models of perturbations and the homogeneous parts.

Now we begin a segment which succinctly summarises an exposition by Baumann[7], with a handful of additions to specialise this introduction for our purposes, particularly from Bertschinger & Ma[18], Brandenberger, Feldman & Mukhanov[20].

One strength of this model is that Fourier modes

$$X_{\mathbf{k}}(t) : = \int X(t, \mathbf{x}) e^{-2\pi i \mathbf{k}\cdot\mathbf{x}} \quad \mathrm{d}\mathbf{x},$$

where the continuously variable $\mathbf{k}$ is often called a **wave-vector**, vary independently of each other, so can be studied separately. Additionally, perturbations to scalar quantities (classified by generally transforming trivially under spatial rotations) can be considered separately to other classes (for the proof see [7]). As a result, we can choose the so-called Newtonian gauge for our perturbation to the metric [18, pp. 7] in order to study scalar perturbations, in which case many important quantities are in terms of $k : = |\mathbf{k}|$. Why perturbations to the metric? The dynamics of the inflaton field are derived from the metric of the space; both the Friedmann and fluid equations follow from Einstien's field equations, and the stress-energy-momentum tensor is derived from the inflaton field ϕ. Thus, we can capture the altered dynamics by studying perturbations to ϕ and the metric, the latter being

$$\mathrm{d}s^2 = -(1 + 2\Phi)\mathrm{d}t^2 + a^2 \left((1 - 2\Psi)\mathrm{d}x^i \mathrm{d}x_i\right)$$

in the Newtonian gauge. $\Phi = \Psi$ when anisotropic stresses are neglected.
A caveat is that many 'phenomena' are merely artefacts of gauge choice - our remedy will be to study gauge invariant quantities only, for instance the comoving curvature perturbation $\mathcal{R}(\mathbf{x})$ as a gauge invariant form of Ψ. Studying the different modes $\mathcal{R}_{\mathbf{k}}$, one finds the correlation to be described by

$$\langle \mathcal{R}_{\mathbf{k}} \mathcal{R}_{\mathbf{k'}} \rangle = (2\pi)^3 P_{\mathcal{R}}(k) \delta(\mathbf{k} + \mathbf{k'}).$$

Such defines the **power spectrum** $P_{\mathcal{R}}$ of $\mathcal{R}$. Thus, we define a parameter which determines the local shape of the power spectrum, the **scalar spectral index**, by

$$n_s - 4 = \frac{\mathrm{d} \log P_{\mathcal{R}}}{\mathrm{d} \log k}. \tag{16}$$

By locally modelling $P_{\mathcal{R}} \sim k^x, (n_s - 4)$ is the exponent x, though usually one considers $n_s - 1$ (the quantity is usually written in terms of an explicitly dimensionless version of the power spectrum).

We also get an analogous power spectrum P_h for tensor perturbations to the spatial part of the metric; as a perturbation to the FLRW metric this appears as

$$\mathrm{d}s^2 = -\mathrm{d}t^2 + a^2[g_{ij} + h_{ij}]\mathrm{d}x^i \mathrm{d}x^j.$$

In general, this gives rise to gravitational waves. Again, tensor perturbations are characterised by their transformation under spatial rotations and may be considered in separately

to other classes. Due to the fact that we are considering coordinate changes as the possible gauge transformations h_{ij} is gauge invariant [2, 00:19:12]. Now we define the **tensor-to-scalar ratio** as

$$r = \frac{P_h}{P_{\mathcal{R}}}.$$

r also gives a measure of the energy scale of the early Universe with $r \geq 0.01$ being an indication of GUT energy scales.

Measurements which place bounds on r and n_s come from a particular scale of perturbation. Fixing wave-vector $\mathbf{k}$ (of appropriate norm, for instance 0.002Mpc^{-1} [4]) there is a time during inflation at which $k = aH$. By definition of inflation, $k < aH$ for some period of time afterwards. It can be shown that the amplitude of $\mathcal{R}_{\mathbf{k}}$ remains fixed while $k < aH$, ultimately meaning that predictions of r an n_s *based on wavelength k data* correspond to conditions at the time during inflation when $k = aH$. Thus, a choice of t determines values of n_s and r, which are principally functions of k, namely

$$n_s = 1 - \frac{4\varepsilon - 2\eta}{1 - \varepsilon}, \tag{17}$$

$$r = 16\varepsilon. \tag{18}$$

where ε and η are evaluated at t such that $k = aH(t)$. This ends our summary of Baumann's exposition.

4.1 Foundational methodology

From the 2018 Planck mission (in this dissertation we use [3]), we have empirical restrictions on r and n_s (see figure 4). A result of the data collected from the Planck missions is the expectation that these quantities *do not depend on $\boldsymbol{k}$ at all*, or at least negligibly in the range of wave-vectors probed by the Planck satellite. Later, we will see different models which appear to predict a dependence of n_s and r on time (which will be parametrised by N), but we will interpret this in the usual sense for now[7] as an inspecificity of prediction. Given this, we will work towards narrowing down the variety of dynamics which agree with Planck observations.

In particular we ask that *predictions corresponding to as much inflation as sufficient, $N \gtrsim 60$, agree with the data as well as possible.*

4.2 A comparison of SR inflation with Planck data

For now, we consider potentials of the form $V = V_0\phi^m$ for $m > 0$, called **monomial potentials**.

[7] See conclusion, areas of interest.

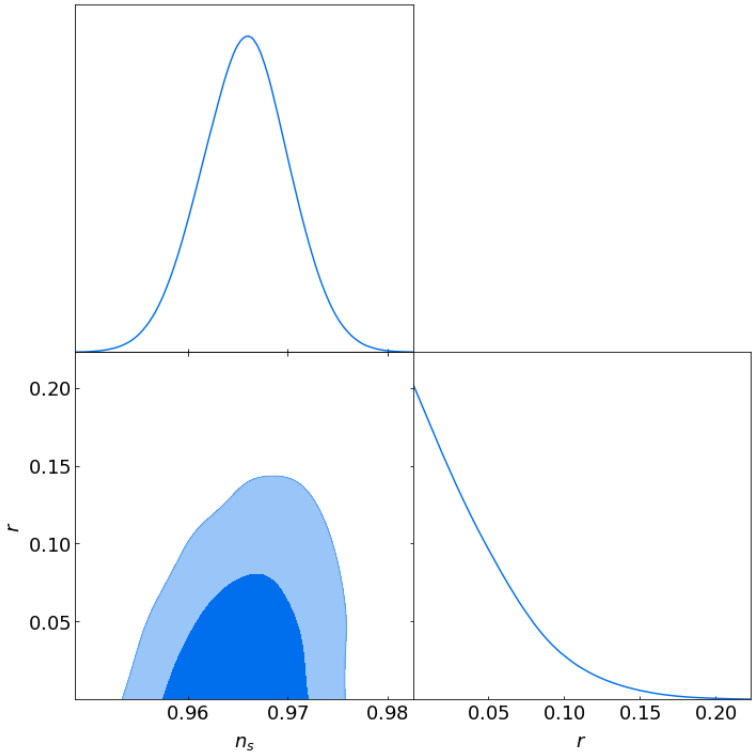

Figure 4: We use our main data source [3] and python's specialised `getdist` functions to produce this triangle plot (see `https://github.com/jacb1729/DynamicsofCosmoinflation2021`, *SRcode for dissertation.ipynb*), illustrating the shape of (marginal) probability distributions of observables r and n_s as well as the 68% and 95% confidence intervals of their joint distribution. The tools we develop in this dissertation will allow us to evaluate specific models against these restrictions.

We consider first SR inflation. If $V = V_0\phi^m$, then $V' = mV_0\phi^{m-1}$. Under the SR regime (using the approximations listed in 3.1), ε and η are given by

$$\varepsilon = \frac{m^2}{2\phi^2}, \quad \eta = \frac{m(m-1)}{\phi^2}. \tag{19}$$

Under SR conditions we can calculate N exactly and parametrise ϕ, r and n_s by it;

$$N = \int_{\phi_0}^{\phi} \frac{V}{V'} \quad \mathrm{d}\phi = \int_{\phi_0}^{\phi} \frac{\phi}{m} \quad \mathrm{d}\phi.$$

Using $\varepsilon < 1 \Leftrightarrow$ inflation is occurring, we can approximate N by setting $\varepsilon(\phi_0) = 1$ and solving for ϕ_0,

$$\phi_0 = \frac{m}{\sqrt{2}}.$$

$$\text{Thus,} \qquad N = \int_{\frac{m}{\sqrt{2}}}^{\phi} \frac{\phi}{m} \mathrm{d}\phi = \frac{\phi^2}{2m} - \frac{m}{4}. \tag{20}$$

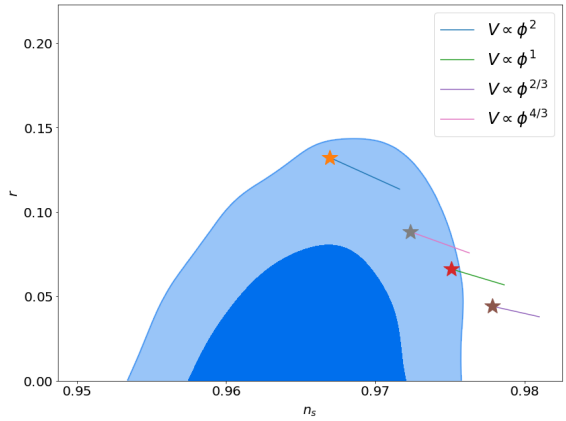

Figure 5a: Plot of the SR inflation results for the potentials of the form $V = V_0\phi^m$ shown (see *SRcode for dissertation.ipynb*), $60 < N < 70$. Inflation is predicted to last for time corresponding to $N \gtrsim 60$, so stars are plotted at points corresponding to $N = 60$.

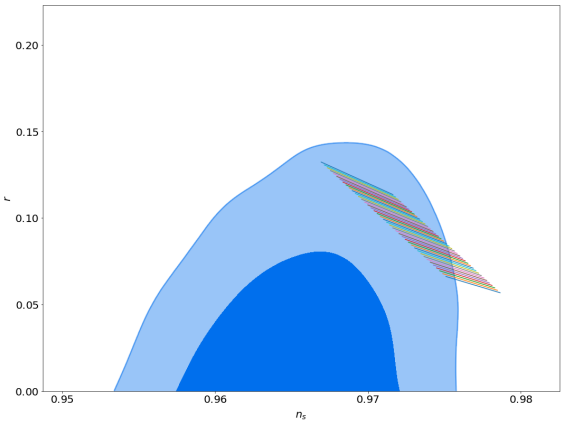

Figure 5b: A plot like the left figure but with a greater density of m values; $m \in [1.5, 2]$ give $N \in [60, 70]$ values of (n_s, r) inside the 95% confidence interval, for example. Each line segment colour indicates an interval of particular m value.

There is a freedom of gauge in this problem - ϕ only enters relevant quantities as ϕ^2, so we need only note that

$$\phi^2 = 2m(N + \frac{1}{4}m). \tag{21}$$

Now we may rewrite using (21)

$$\varepsilon = \frac{m}{4}\frac{1}{N + \frac{1}{4}m},$$
$$\eta = \frac{m-1}{2}\frac{1}{N + \frac{1}{4}m}.$$

Using (18),

$$r = \frac{4m}{N + \frac{1}{4}m}, \tag{22}$$
$$n_s = 1 - \frac{\frac{1}{2}m + 1}{N + \frac{1}{4}m}. \tag{23}$$

We plot this prediction for sensible N values (figure 5) to test the validity of the SR paradigm as a model against corresponding predictions from the Planck experiment [3] (see `http://pla.esac.esa.int/pla/#cosmology`). The code used to produce these plots composes *SR code for dissertation.ipynb* which can be viewed at `https://github.com/jacb1729/DynamicsofCosmoinflation2021`.

The interval of (n_s, r) values deforms linearly with m, so a plot like figure 5 tells us that, in this model, $m \in [1.5, 2]$ (for example) are probably the among the more representative

potentials. For fixed N, by (18), (19),

$$r = \frac{-16Nn_s}{2N-1} + \frac{N-1}{2N-1}$$

5 Simulations of HJ inflation

Once again, let $V = V_0\phi^m$ for $m > 0$. We first set up the study of the dynamics given by

$$H'^2 - \frac{3}{2}H^2 = -\frac{1}{2}V.$$

We will not need to consider negative parts of such potentials, i.e the $\phi < 0$ parts for $V_0 \geq 0$. Thinking about the H' vector field in the $\phi - H$ plane, say $\dot{\phi} < 0$. $H' > 0$, so one can show that a point starting with $\phi < 0$ evolving forwards in time in $\mathfrak{D}_{\text{eff}}$ will exit this set via the $\varepsilon = 0$ boundary, which doesn't predict and end of inflation. Even when $\dot{\phi} > 0$ we will not get a sufficient amount of inflation. Noting the definition of $\mathfrak{D}_{\text{eff}}$ as in (15), $(0, H) \notin \mathfrak{D}_{\text{eff}}$ for all $H \in \mathbb{R}$ for monomial potentials, so the sign of ϕ can not change, there appears to be little reason to consider $\phi < 0$.
The notable quantities (a derivation of η is included in Appendix 1), as before, are

$$\varepsilon = 2\left(\frac{H'}{H}\right)^2, \tag{24}$$

$$\eta = 2\varepsilon - 4\frac{H''}{H}, \tag{25}$$

$$r = 32\left(\frac{H'}{H}\right)^2, \tag{26}$$

$$n_s = 1 - \frac{8H''H}{H^2 - 2H'^2} = 1 - \frac{8H''H}{V - 2H^2} \tag{27}$$

where we can evaluate derivatives of H to a function of H and ϕ using (11).

5.1 The challenge of analytic solutions

Here we briefly motivate looking for numerical as opposed to analytical solutions.
There are only a few notable scenarios for which exact solutions are known - the general ϕ^m potential that we are considering is not one of these. One trivial case is that of $V_0 = 0$, giving $H \propto e^{\lambda\phi}$ for some $\lambda \in \mathbb{R}$, but more notably is a class of exponential potentials as in [12], a generalisation of the classic Power Law inflation [17, Chapter 3].

One method is to reformulate the problem; one can consider the equation borne of $\frac{\mathrm{d}\varepsilon}{\mathrm{d}\phi}$ and the fact that $H^2 = \frac{V}{3-\varepsilon}$, to get

$$\frac{\mathrm{d}\varepsilon}{\mathrm{d}\phi} = \left(\sqrt{2\varepsilon} - \frac{V'}{V}\right)(3 - \varepsilon).$$

I have found that using an integrating factor then integrating by parts leads to a tautological statement unfortunately, regardless of the C^1 potential V chosen.

It is noteworthy that ϕ and H are not conjugate variables (in the Hamiltonian sense), but perhaps this is something we are hoping for [22]; we want a dynamics with an 'attractor' in some sense. The motivation for inflation can be phrased as requiring a larger set of initial ρ and $\dot{\rho}$ states to lead to the smaller set at the end of inflation, but requiring a Hamiltonian dynamics, a volume preserving dynamics, places restrictions on the rate of convergence. Furthermore, there can be no attracting sets in Hamiltonian dynamics because of this volume preservation property. In summary, we can't rely on our dynamics being Hamiltonian in the search of analytic solutions.

5.2 Prototype numerical scheme to solve the HJ equation

We are thus motivated to solve the HJ equation(11) numerically. The result of numerical integration should be a curve in the $\phi - H$ plane phase space $\mathfrak{D}_{\text{eff}}$ - if the scheme employed is appropriate we do not expect the choice of $\dot{\phi} > 0$ or $\dot{\phi} < 0$ to affect our result.

Choosing $\dot{\phi} < 0$ gives $H' > 0$ by (10). Here I outline a prototype numerical integration scheme (presented in figure 7) which forms a good basis but is insufficient, then proceed to produce an acceptable improvement later.
The standard integrator[8] one employs for its mix of accuracy and speed is the Runge-Kutta scheme of 4^{th} order (RK4) with fixed step-size. For an ODE $\frac{\mathrm{d}y}{\mathrm{d}x} = f(x, y)$, this scheme produces a finite sequence of points $\{(y_n, x_n)\}_{n=0}^{n=T}$ for a step-size h such that

$$\begin{aligned}
x_{n+1} &= x_n + h, \\
K_{n_1} &= f(x_n, y_n), \\
K_{n_2} &= f(x_n + \frac{1}{2}h, y_n + \frac{1}{2}K_{n_1}), \\
K_{n_3} &= f(x_n + \frac{1}{2}h, y_n + \frac{1}{2}K_{n_2}), \\
K_{n_4} &= f(x_n + h, y_n + K_{n_3}), \\
y_{n+1} &= y_n + h\frac{K_{n_1} + 2K_{n_2} + 2K_{n_3} + K_{n_4}}{6}.
\end{aligned}$$

Higher order RK schemes are extensions of this idea - a series of approximations of the gradient f on $[x_n, x_n + h]$ are made, and in each gradient approximation the preceding gradient approximation is used to approximate intermediate y values necessary for the gradient approximation.

Here are two ways we should track inflation. First, by definition, $\varepsilon < 1$ defines the period of inflation, so we desire this as well as $\varepsilon = 1$ at the end. Second, we will parametrise time

[8] I will use "integrator" to refer to the recursion relation which is the crux of the broader algorithm, the latter being what I call the "integration scheme"

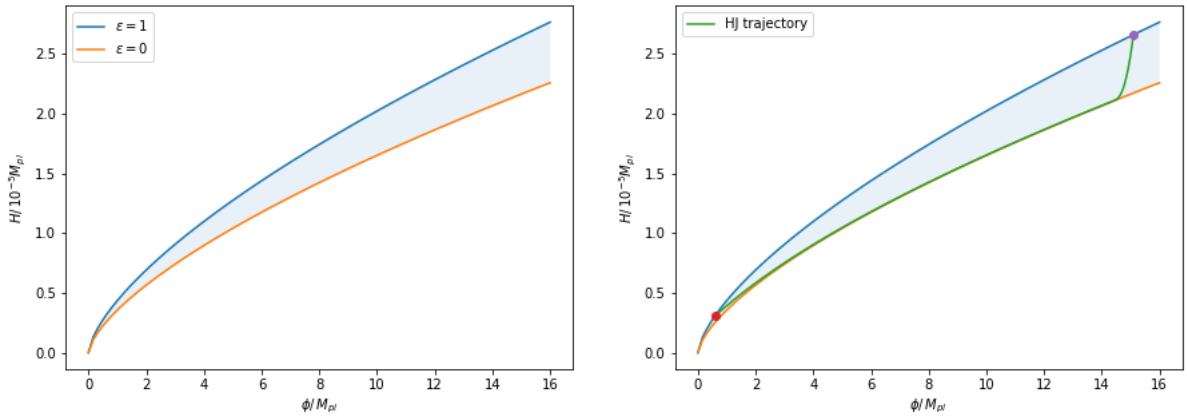

Figure 6: An example of the effective domain of the HJ equation (11) in the context of inflation (with potential $V(\phi) = V_0\phi^{\frac{4}{3}}$ in this case); this domain $\mathfrak{D}_{\text{eff}}$ is shaded with the ε boundaries highlighted (and, on the left, labelled). On the right, a trajectory generated by the scheme we are motivating here is plotted with its endpoints highlighted; note that this trajectory closely approaches but does not touch the $\varepsilon = 0$ boundary, a behaviour whose existence we will deduce exists for $V = V_0\phi^m$ potentials with $m > 0$. An interested user can produce a plot of the domain of their choice at *domains.ipynb*.

by N, which is useful because of the immediate physical implications of so many e-folds having passed and, as a result, the known lower bounds on N in various models ([4], [17]). The idea will be to produce a curve in $\mathfrak{D}_{\text{eff}}$, with the $N = 0$ endpoint along the $\varepsilon = 1$ boundary (see figure 6), with $N \gtrsim 60$. We will discuss later why the curve can usually be extended further to have $\varepsilon = 1$ at the other endpoint for $V_0\phi^m$ potentials.

Simulations will be between the end of inflation and a final time (which is varied between executions) N_b. N_b is the earliest N value associated with a point along the trajectory in question (in figure 7 this is `NMAX`), what for a traditional variable trajectory would be the initial time. More generally, we will denote the value of quantity Q predicted to coincide with N_b by Q_b. Using Planck 2018's *Constraints on inflation*, we have $H_b \lesssim 2.5 \times 10^{-5}$ also [4, eqn 33], which will help us narrow down possible trajectories. Given H_b, we have restrictions on V_0 and ϕ_b by the shape of $\mathfrak{D}_{\text{eff}}$.

Our method is to choose sensible initial ϕ and V_0 values for initial $H \lesssim 2.5 \times 10^{-5}$, employ our choice of numerical integrator to solve (11) from the time corresponding to initial parameter choices to the time at the end of inflation, and finally integrate backwards in time, which we refer to as **backwards integration**, to get the N parametrisation and the full trajectory, corresponding to the desired amount of inflation. More specifically, my first attempt at a method is summarised in figure 7.

Using this method, there are some issues, the more obvious of which is that H_b can be greater than the constraint of $\lesssim 2.5 \times 10^{-5}$ after backwards integration. I will note 2

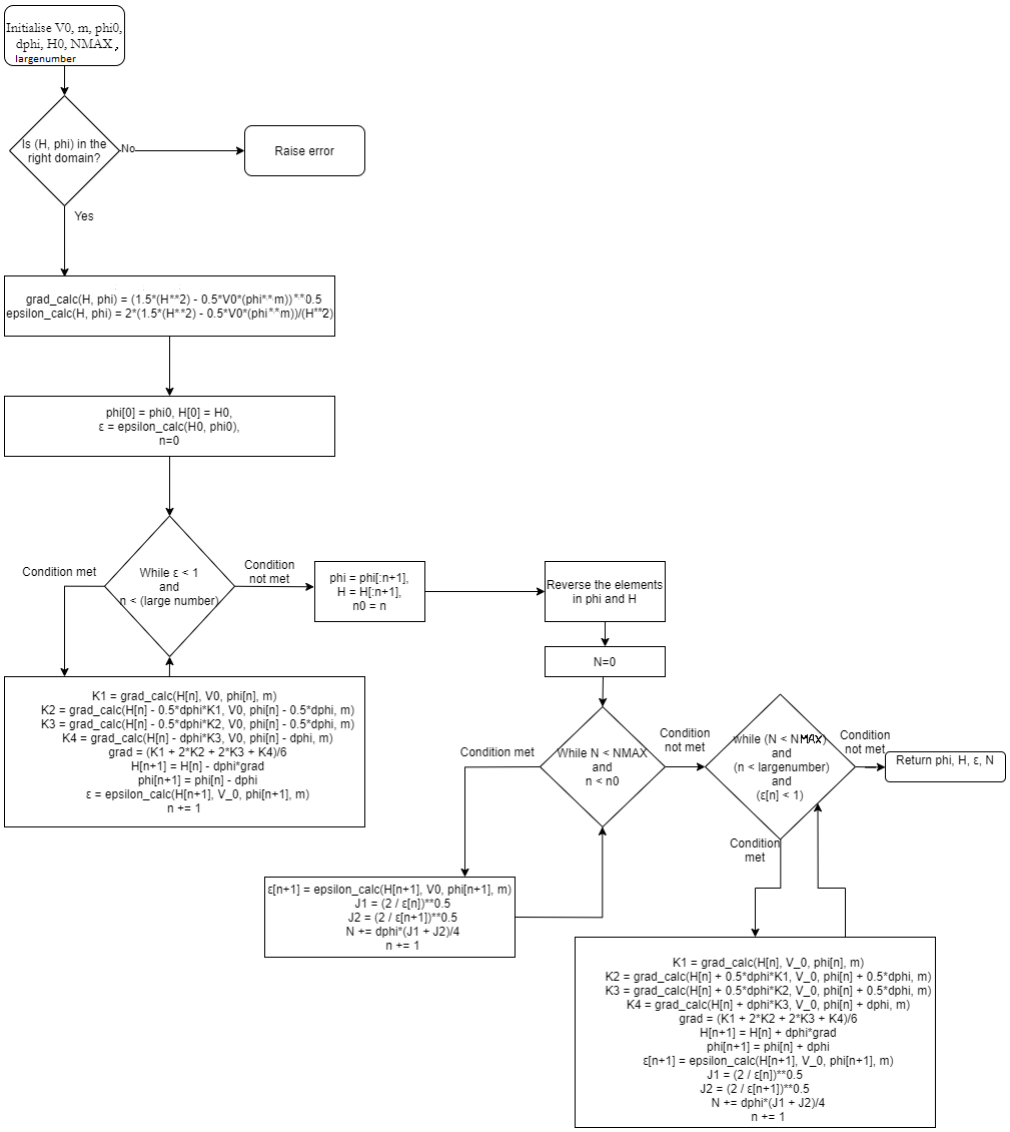

Figure 7: The key ideas of the prototype algorithm are summarised here. The pseudocode is closest in syntax to python, the language of code from which I have extracted this diagram.

solutions, though the first will suffice in most cases:

1. Prescribing a choice of V_0 and initial ϕ gives rise to a choice of initial ε. A trajectory in the $\phi - H$ plane implicitly determines a trajectory in the $\phi - \varepsilon$ plane[9], for which ε approaches 1 via a continuous curve from the below. Provided you are willing to take an experimental approach (as am I), choosing V_0 and initial ϕ such that the initial value of ε is just a little less than 1 will ensure that only a little correction via backwards integration is necessary, thus minimising deviation of H_b from the initial H given (see figure 8). The caveat is that one can not always extend a trajectory backwards in time to the $\varepsilon = 1$ boundary, so this strategy of starting values choices will not give rise to all solutions.

2. In the case that one's major concern getting a precise trajectory for *some* potential over getting a precise trajectory for a particular choice of potential, one can rescale the solution given after backwards integration to give H_b as desired at the expense of changing the potential. Suppose we get a value H_b after employing the scheme, but we want H to take value $\tilde{H}_b$ at the beginning of inflation. Rescale (11) as follows:

$$\left(\frac{\tilde{H}_b}{H_b}H'\right)^2 - \frac{3}{2}\left(\frac{\tilde{H}_b}{H_b}H\right)^2 = -\frac{1}{2}\left(\frac{\tilde{H}_b}{H_b}\right)^2 V.$$

   We thus have our best guess at the trajectory starting at the experimentally justified initial H_b we have chosen for a potential $\left(\frac{\tilde{H}_b}{H_b}\right)^2$ times larger than the potential put chosen before employing the scheme; under this scaling, $\varepsilon \to \varepsilon$ and $N \to N$.

A second, less evident but more fatal issue is that a fixed step-size scheme (with too large step-sizes) tends to lead to an incorrect prediction that $\varepsilon < 0$ during inflation. Indeed, under our assumption of $\dot{\phi} \neq 0$ we need $\varepsilon > 0$. Implicit in the prediction $\varepsilon < 0$ is that the trajectory we approximate via this scheme moves to a point in the $\phi - H$ plane with $\frac{3}{2}H^2 - \frac{1}{2}V < 0$ (a point below the $\varepsilon = 0$ curve on a plot like figure 6 for example). Not only is this trajectory flawed in an obvious theoretical manner but it causes the integration scheme to fail too. Considering the dynamics of the HJ equation in terms of separatrices will distinguish two mutually exclusive cases of this failure.

5.3 Separatrices of the HJ equation

It is well known ([17, chapter 3] for example) that a small perturbation in the Hubble parameter will decay over time; let H_0 solve (11) and let δH be a small perturbation of H_0 such that $H := H_0 + \delta H$ solves (11). We briefly consider δH at some ϕ corresponding to a value taken by the inflaton field *at a later time*. Linearising (11) with respect to δH

[9]Indeed, as I had noted in motivating the ε ODE in chapter 5.1, under HJ inflation ε as a function of time is almost everywhere locally invertible by the inverse function theorem.

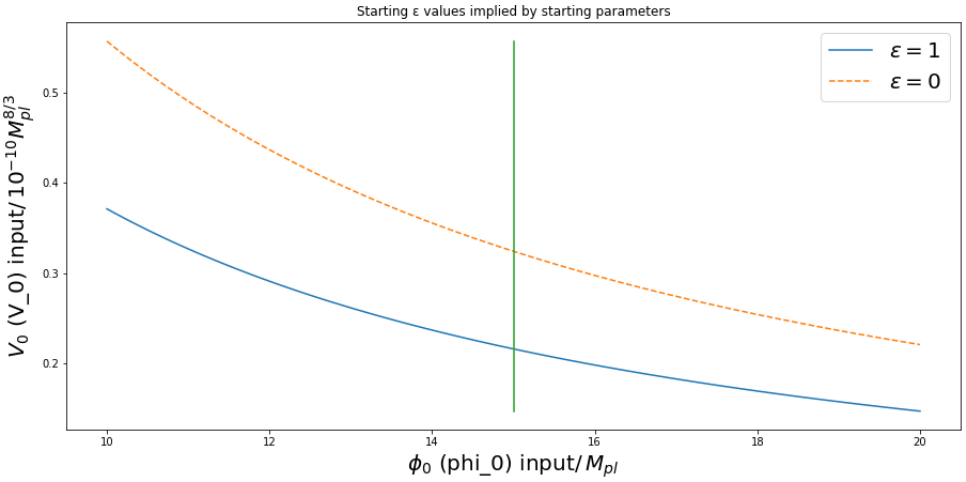

Figure 8: The starting input coefficient V_0 for potential $V_0\phi^m$ and starting values ϕ_0, H_0 imply a starting ε value; here we have plotted the curves in $\phi_0 - V_0$ space which determine starting ε values of 0 and 1 for $H_0 = 2 \times 10^{-5}$, $m = \frac{4}{3}$. Such plots can be produced in one cell in the notebook *Numerical HJ simulations.ipynb*.

gives

$$\begin{aligned} H_0'(\delta H)' \simeq & \frac{3}{2} H_0 \delta H \\ \delta H(\phi) \simeq & \delta H(\phi_0) \exp\left(\frac{3}{2}\int_{\phi_0}^{\phi} \frac{H_0}{H_0'} \quad \mathrm{d}\phi\right). \end{aligned}$$

As $H' \propto -\dot{\phi}$, either $\frac{1}{H_0}\mathrm{d}\phi$ is a negative measure or $\phi < \phi_0$. Moreover, the integrand is of magnitude $\sqrt{\frac{2}{\varepsilon_0}}$, so the rate of decay of δH is at least[10] $e^{\frac{3}{\sqrt{2}}\phi}$.

Reversing this, nearby solutions to (11) separate as ϕ increases. Recall that we are working with $\dot{\phi} < 0$ but results are similar in general using symmetry of (11). Rephrasing equation (38) in [5],

$$H(\phi) = H(\phi_0) \exp\left(\int_{\phi_0}^{\phi} \sqrt{1 - \left(\frac{V}{3H}\right)^2}\, \mathrm{d}\phi\right)$$

so two solutions to (generally distinct) IVPs of (11) H_1, H_2 separate according to

$$\frac{H_2}{H_1}(\phi) = \frac{H_2}{H_1}(\phi_0) \exp\left(\int_{\phi_0}^{\phi} \sqrt{1 - \left(\frac{V}{3H_2}\right)^2} - \sqrt{1 - \left(\frac{V}{3H_1}\right)^2}\, \mathrm{d}\phi\right). \tag{28}$$

[10] In standard notation this would be $\Omega(e^{\frac{3}{\sqrt{2}}\phi})$ but I have resigned this to a footnote to avoid clashing with notation for the density parameter.

These results will be useful to show the existence of separatrix solutions to (11). For the remainder of this subsection we will summarise the ideas needed from [5], an article by Álvarez et al which concerns solutions to the HJ equation on $\mathfrak{D}$, with some edits to terminology and formulation, but first I will focus on and prove a passing statement from said article:

Lemma 1. Let V be differentiable, and say there exist $C > 0$ and $\phi_0 \in \mathbb{R}$ such that $V'(\phi) \geq C$ for all $\phi \geq \phi_0$. We conclude that there is an $d \in \left(\sqrt{\frac{1}{3}V(\phi_0)}, \infty\right]$ such that any solution H to the HJ equation (11) on $\mathfrak{D}$ with potential V such that $H(\phi_0) < d$ exits $\mathfrak{D}$ via the $\varepsilon = 0$ boundary.

Proof. Curves in the $\phi - H^2$ plane of constant H' are translations of the line $H^2 = \frac{1}{3}V(\phi_0)$. Consider in particular the curve of $H' = \frac{1}{2}C$, i.e the curve $H^2 = \frac{1}{3}V + \frac{1}{6}C^2$ (figure 9, right). By mapping the open set $\mathcal{O}$ defined as the area in strictly between $H^2 = \frac{1}{3}V$ and $H^2 = \frac{1}{3}V + \frac{1}{6}C^2$ under the (continuous) map $f : \bar{\mathcal{O}} \to \mathbb{R}^2$ defined $f(\phi, \varphi) = (\phi, \sqrt{\varphi})$,

- Line segments of constant ϕ map to line segments of constant ϕ by continuity.
- $x \mapsto \sqrt{x}$ is an increasing bijection on $\mathbb{R}_0^+$, so curves in $\mathcal{O}$ map bijectively to curves under the $H' = C$ contour in the $\phi - H$ plane (which is how we interpret the codomain).

Set L_C to be the straight line segment in the $\phi - H^2$ plane between $(\phi_0, \frac{1}{3}V(\phi_0))$ and $(\phi_0, \frac{1}{3}V(\phi_0) + \frac{1}{6}C^2)$. Solutions to (11) on $\mathfrak{D}_{\text{eff}}$ with $(\phi_0, H(\phi_0))$ in $f(L_C)$ (which is the line between points of ϕ value ϕ_0 on the $H' = 0, H' = \frac{1}{2}C$ contours in $\mathfrak{D}_{\text{eff}}$) must exit via the $\varepsilon = 0$ boundary of $\mathfrak{D}_{\text{eff}}$ because they lie in $f(\mathcal{O})$. Indeed, $H'(\phi) < \frac{1}{2}C \, \forall \phi \geq \phi_0$ for any such solution H, so

$$H(\phi) - V(\phi) = H(\phi_0) - V(\phi_0) + \int_{\phi_0}^{\phi} (H' - V')\mathrm{d}\phi \leq H(\phi_0) - V(\phi_0) - \frac{1}{2}C(\phi - \phi_0).$$

□

We conclude conditions sufficient for the existence of solutions of **type A** variety. Before the following definition, we note a class of families of IVPs which we need to consider, namely the family of IVPs of the HJ equation for $\phi > 0$ with chosen initial point $\phi_0 > 0$, chosen domain contained in $\mathfrak{D}$, each member of which family is specified by the value of $H(\phi_0)$.

Definition 2. A solution to an IVP for the HJ equation (11) defined by specifying $H(\phi_0)$ and the domain (contained in) $\mathfrak{D}$ is of **type A** iff it exits the domain within finite time via the $\varepsilon = 0$ boundary.

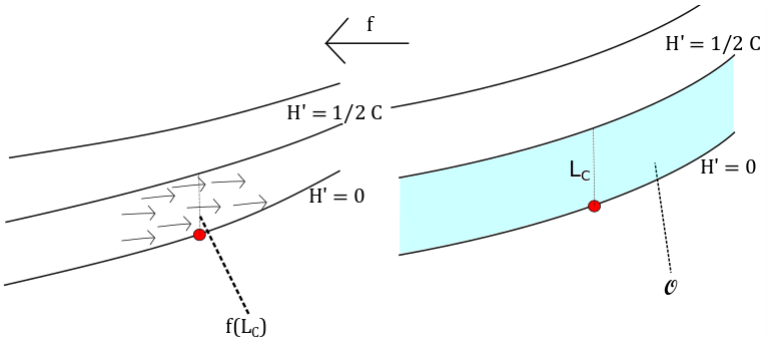

H.png

Figure 9: The proof of the lemma focuses on the fact that f maps vertical line segments in the $\phi - H^2$ to the corresponding line segment in the $\phi - H$ plane in such a manner that we can select a length of a vertical line segment, one which like L_C is a segment between the point $(\phi_0, \frac{1}{3}V(\phi_0))$ on the $\varepsilon = 0$ boundary and a point above it, so that all points along it give rise to solution curves of the HJ equation (11) which exit $\mathfrak{D}_{\text{eff}}$ via the $\varepsilon = 0$ boundary. Point $(\phi_0, \frac{1}{3}V(\phi_0))$ and its image under f are highlighted in red.

The conditions of the hypothesis of lemma 1 are satisfied are satisfied by $V = V_0\phi^m$ potentials with $\phi_0 = \phi_b > 0$.

If the supremum of possible choices of d for a particular ϕ_0, quantities denoted as in the lemma, is finite then there are solutions to the IVP on $\mathfrak{D}$ which are defined for all $\phi > \phi_0$, solutions of **type B** on $\mathfrak{D}$. These are defined as solutions to members of the family of IVPs (as posed in the definition of type A solutions) for which the specified $H(\phi_0) > d_s$ [11], where d_s is the supremum choice of d for this fixed ϕ_0, i.e this family. We call d_s for the IVP starting at ϕ_0 the **separatrix value** for ϕ_0. Type B solutions grow exponentially in the large ϕ limit as a result of equation (28). Finally, a **separatrix** for the IVP on $\mathfrak{D}$ is the unique solution to the HJ equation which is neither type A nor type B, i.e the solution with $H(\phi_0) = d_s$.

To define such behaviour classes for IVPs on $\mathfrak{D}_{\text{eff}}$, we will also require that $(\phi_0, H(\phi_0)) \in \mathfrak{D}_{\text{eff}}$, which means d_s must be sufficiently small. For example, a solution H to the IVP of (11) at initial point ϕ_0 is type-A iff $(\phi_0, H(\phi_0)) \in \mathfrak{D}_{\text{eff}}$ (for the specified potential) and $H(\phi_0) < d_s$.

Definition 3. If a family of IVPs defined as for definition 2 has both type-A (for which $H(\phi_0) < d_s$) and type-B solutions (for which $H(\phi_0) > d_s$), then the solution to the IVP with $H(\phi_0) = d_s$ is the **separatrix** for that family, where d_s is the separatrix value for that family.

The separatrix is what the literature on single field inflation often calls an *attractor*.

[11] We synthetically exclude the separatrix from this class.

5.4 Corresponding dynamics in the $\phi - \dot{\phi}$ plane

In the next subsection, I will describe the relevance of these solution classes to numerically solving the HJ equation. First, I will introduce a dual perspective in our set-up.

By $\dot{\phi} = -2H'(\phi)$, there is a diffeomorphism between any quadrant of the $\phi - H$ plane and some quadrant of the $\phi - \dot{\phi}$ plane which maps solution curves to HJ equation in the $\phi - H$ plane to solution curves to the HJ equation in the $\phi - \dot{\phi}$ plane (injectively). Without considering domains currently, which is what we have done for the $\phi - H$ plane, we can produce a superset of solutions in an dynamics in the $\phi - \dot{\phi}$ plane, equivalent to the HJ equation apart from domain choice.

Next we generalise an idea in [19, pp. 236]. Substituting the formula for H given by equation (7) into (8),

$$\ddot{\phi} + \sqrt{3}\dot{\phi}\sqrt{\frac{1}{2}\dot{\phi}^2 + V} + V' = 0. \tag{29}$$

By assuming $\dot{\phi} \neq 0$, at least locally, we may channel the inverse function theorem to write $\dot{\phi}$ as a function of ϕ, in which case $\ddot{\phi} = \dot{\phi}\frac{\mathrm{d}\dot{\phi}}{\mathrm{d}\phi}$, so we get

$$\frac{\mathrm{d}\dot{\phi}}{\mathrm{d}\phi} = -\frac{1}{\dot{\phi}}\left(\sqrt{3}\dot{\phi}\sqrt{\frac{1}{2}\dot{\phi}^2 + V} + V'\right).$$

Conversely, when $|\dot{\phi}| \ll 1$

$$\ddot{\phi} \simeq -V'(\phi), \qquad \frac{\mathrm{d}\dot{\phi}}{\mathrm{d}\phi} \sim -\frac{V'}{\dot{\phi}}, \tag{30}$$

which I will call the **quadrant crossing approximation** (QC). We can easily patch together trajectories across different quadrants by using this picture of the phase portrait when $\dot{\phi}$ is near 0.

Now suppose $|\dot{\phi}| \gg V_0\phi$, a non-inflationary regime known as **kinetic dominance** which helps us draw a portion of the phase portrait for (29). This gives an approximation (perfect in the limit implied by the assumption) of

$$\frac{\mathrm{d}\dot{\phi}}{\mathrm{d}\phi} \simeq \sqrt{\frac{3}{2}}\dot{\phi}, \text{ so } \dot{\phi} \simeq Ce^{\sqrt{\frac{3}{2}}\phi}.$$

We find that $\dot{\phi}$ decays much faster than ϕ for $\dot{\phi} < 0$, and grows much faster for $\dot{\phi} > 0$, for large $\dot{\phi}$. An example of the phase portrait is shown in figure 10. This general shape will be useful to bear in mind the shape a trajectory will likely take away from the separatrix.

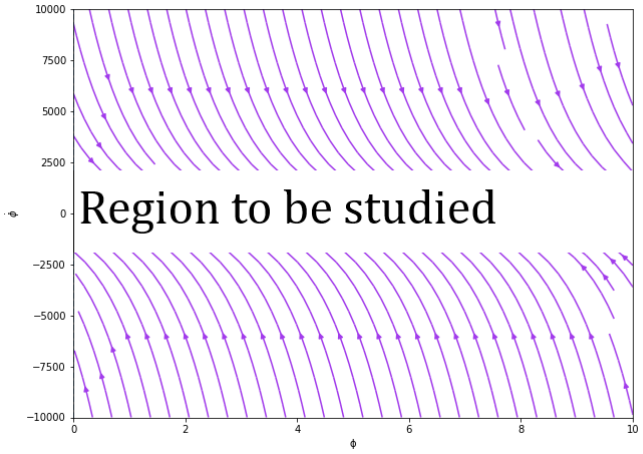

Figure 10: The phase portrait for $|\dot{\phi}| \gg V_0\phi$, generated in python by code like that in *phase space limits.ipynb* in the repository for this dissertation. We have yet to study the region corresponding to inflation, but the non-inflationary information gives 'boundary conditions' on the trajectories for larger ε values.

5.5 An improved numerical scheme for the HJ equation

For monomial potentials, there necessarily exist type-A solutions (the lemma can be easily extended to work for $m \in (0, 1)$, or more generally for $V'(\phi) \geq C(B)$ for all $\phi \in [\phi_0, B]$ if we can choose B free of upper bound). Thus, for type-A solutions to monomial potential IVPs, crossing the corresponding $\varepsilon = 0$ contour in the $\phi - \dot{\phi}$ plane is unavoidable. Unchallenged, this leads unavoidably to $\varepsilon < 0$ errors in the numerical scheme for the HJ equation. On the contrary, any type-B solutions should have a positive minimum value taken by the corresponding ε trajectory in the $\phi - \varepsilon$ plane, so $\varepsilon < 0$ errors seems more easily avoidable.

Though we do not currently know where the attractor is, experimentation tells us that much of the attractor should correspond to small values of ε, which in the $\phi - H$ plane is within $\mathfrak{D}_{\text{eff}}$ and the locality of the $\varepsilon = 0$ boundary. This is supported by [9], as the scale of considerations well-modelled by monomial potentials is so-called *large field*, because SR solutions are expected to be local attractors. One result will be an improvement on this estimation of attractor solutions as only vaguely SR solutions.

Thus, our solution to the $\varepsilon < 0$ error for type B solutions is motivated by assuming the separatrix is very close to the $\varepsilon = 0$ boundary. The error is caused by unwittingly crossing the separatrix, so we will change the step size while ε is small to avoid this. Suppose that, at step n of the scheme approximating a type B solution is at the point $p_n = (\phi_n, H_n) \in \mathfrak{D}_{\text{eff}}$. Now we suppose that $H'(p_n)$ is a good approximation of the gradient which will be used

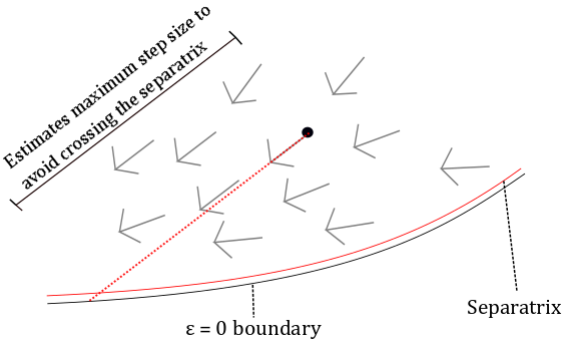

Figure 11: Consider a point $p_n \in \mathfrak{D}_{\text{eff}}$ above the separatrix, evolving along an integral curve of the vector field H'. Our prototype scheme approximates its local evolution by using a weighted average of its current H' value and some successive approximations (via RK4) to determine a sensible gradient approximation for the integral curve. Our improved scheme uses H' at p_n as a first gauge of the local integral curve gradient, approximates the step-size which would evolve p_n across the separatrix using this first gradient estimate and by approximating the separatrix to be at the $\varepsilon = 0$ boundary, and chooses a step-size which will hopefully avoid this, then proceeds as before.

to calculate $p_{n+1} = (\phi_{n+1}, H_{n+1})$, i.e *we suppose*

$$K_{n1} \approx \frac{K_{n_1} + 2K_{n_2} + 2K_{n_3} + K_{n_4}}{6} \tag{31}$$

comparing with the description of RK4 earlier. The motivation for this approximation is as follows: the error we are trying to avoid is the approximation of a type B solution curve passing over the separatrix, which should itself define a distinct solution to the HJ equation. A likely source of separatrix crossing error is that too large a step is taken while the trajectory is turning from virtually vertical to alongside the separatrix, a process during which the value of H' rapidly decreases, so for n^{th} step p_n occurring during this turning process the approximation H' should be strictly conservative, that is we expect $K_{n1} \lesssim \frac{K_{n_1}+2K_{n_2}+2K_{n_3}+K_{n_4}}{6}$.

Now we will choose the step size h_{n+1} so that if we approximate the trajectory as moving along the vector $H'(p_n)$ then this approximate trajectory does not cross the $\varepsilon = 0$ boundary. Also approximating $V(\phi_{n+1})$ by $V(\phi_n)$, we demand

$$H_n - H'(p_n)h_{n+1} > \sqrt{\frac{1}{3}V(\phi_n)}$$
$$\frac{H_n - \sqrt{\frac{1}{3}V(\phi_n)}}{H'(p_n)} > h_{n+1}.$$

The formula is the same for forwards and backwards integration.

A fortunate artefact of earlier work but something we will keep out of the awareness that

the separatrix approximation used above becomes less sensible as the trajectory approaches the separatrix, an expectation that less simple trajectories may require it, and so that the code may be adapted in the future if the HJ equation becomes better understood, we choose step size

$$h_{n+1} = f_n(\varepsilon(p_n))\frac{H_n - \sqrt{\frac{1}{3}V(\phi_n)}}{H'(p_n)}$$

where

$$f_n(\varepsilon) \quad = \quad \begin{cases} h_0\left(\frac{H_n-\sqrt{\frac{1}{3}V(\phi_n)}}{H'(p_n)}\right)^{-1} & \text{large } \varepsilon \\ 0.5 & \text{fairly small } \varepsilon \geq \varepsilon_0 \\ 0.5^{\text{Min}\left(\frac{\varepsilon_0}{\varepsilon},\lambda_{\text{Max}}\right)} & \varepsilon < \varepsilon_0 \end{cases}. \tag{32}$$

for some fixed small ε_0, fixed λ_{Max} in the definition of f (to use a leading abbreviation for f_n). In *Numerical HJ examples.ipynb*, we use $\varepsilon_0 = 0.0001, \lambda_{\text{Max}} = 10$. We calculate a minimum in determining the exponent in the final case to avoid $f \to 0$ as $\varepsilon \to 0$.

The above method is good for type B solutions, but tending towards the $\varepsilon = 0$ boundary for type A solutions is a necessity. A type A solution can be interpreted as a piece of a trajectory in the $\phi - \dot{\phi}$ plane. Say the solution tends a point $p \neq 0$ on the $\varepsilon = 0$ boundary (it must tend to a unique point). An analysis like that in the proof of lemma 1 would reveal that there necessarily exists a solution to (11) with $\phi > 0, \dot{\phi} > 0$ which extends uniquely backwards in time to define a curve with an endpoint p on the $\varepsilon = 0$ boundary. Joining these solutions together at p forms a solution, though not strictly in $\mathfrak{D}$, to (11) which intersects the $\varepsilon = 0$ boundary. Thus, type A solutions determine what I will call **extended solutions**, i.e solutions to (11) which may have $H' = 0$ at some point.
Using (30), provided extended solutions cross the $\varepsilon = 0$ contour at $p \neq 0$, the acceleration of ϕ is non-zero in the locality of p. In the case where we have determined the solution curve in the $\phi > 0, \dot{\phi} < 0$ quadrant and we are extending it to a curve with a piece in the $\phi > 0, \dot{\phi} > 0$, the best approximation of the velocity field near p is usefully written as

$$\dot{\phi}(t) = (t - t_0)\ddot{\phi}(t_0) + \mathcal{O}((t - t_0)^2) = -V'(\phi(t_0))(t - t_0) + \mathcal{O}((t - t_0)^2)$$

where intersection with the $\varepsilon = 0$ contour happens at time t_0. This means that *the extended solution curve crosses the $\varepsilon = 0$ contour in finite time.* This justifies the following simple extension of the numerical scheme; when the trajectory would be about to cross the $\varepsilon = 0$ contour at step n of backwards integration,

$$\dot{\phi}_{n+1} = -\dot{\phi}_n,$$
$$\phi_{n+1} = \phi_n.$$

In the $\phi - \dot{\phi}$ plane this step is just following the small vertical line segment from one side of the $\dot{\phi} = 0$ axis to the other. This is equivalent to, using the formulation (32) in terms of f above,

$$f \to -f, \qquad H' \to -\sqrt{\frac{3}{2}H^2 - \frac{1}{2}V}.$$

To reaffirm, crossing to the new quadrant can be treated in the numerical scheme as, for all succeeding actions in the scheme, taking step $-h$ where one would have taken step h and taking negative H'. An instance of the final scheme is shown in *Numerical HJ examples*.

One subtlety with this scheme is that we want to track time in number of e-folds during backwards integration, even during the **quadrant crossing step**[12] $\phi_0 \to \phi_0, H(\phi_0) \to H(\phi_0)$, $\dot{\phi}_0 \to -\dot{\phi}_0$. However, it is challenging to track N numerically and accurately during this step because ε blows up as $\dot{\phi} \to 0$; we will need to change variables in the integral (14). Bearing in mind (30), the estimate for time passed during the quadrant crossing step is based on the approximations of constant potential $V(\phi) \simeq V(\phi_0)$ and $\ddot{\phi} \simeq -V'(\phi_0)$. Given the constant acceleration, a time of

$$\Delta t = -\frac{2\dot{\phi}_0}{V'(\phi_0)}$$

is estimated to pass during this step; next we convert this to an approximation in number of e-folds passed by using an approximation, whose origin will be made clear in the next chapter (see (36)), of

$$\sqrt{\frac{2}{\varepsilon}} \simeq 2\frac{\sqrt{V(\phi_0)}}{\sqrt{3}\dot{\phi}}.$$

Let the time of the initial state $(\phi_0, \dot{\phi}_0)$ of the scheme be $t_i + \Delta t$, so that state after this sign-switching step (this is occurring during backwards integration) corresponds to a time t_i. The cosmic time period Δt corresponds to a number of e-folds ΔN. In writing $N = \int_\alpha^\beta \sqrt{\frac{2}{\varepsilon}}$ we require α to correspond to the later time (see (14) in the context of its subsection) of the time period N corresponds to, so

$$\begin{aligned}
\Delta N &\simeq \int_{\phi(t_i+\Delta t)}^{\phi(t_i+\frac{1}{2}\Delta t)} \frac{\sqrt{V(\phi_0)}}{\sqrt{3}(-\dot{\phi})} \quad \mathrm{d}\phi + \quad \int_{\phi(t_i+\frac{1}{2}\Delta t)}^{\phi(t_i)} \frac{\sqrt{V(\phi_0)}}{\sqrt{3}(-\dot{\phi})} \quad \mathrm{d}\phi \\
&= \left(\int_{t_i+\frac{1}{2}\Delta t}^{t_i+\Delta t} + \int_{t_i}^{t_i+\frac{1}{2}\Delta t} \right) \frac{\sqrt{V(\phi_0)}}{\sqrt{3}} \quad \mathrm{d}t \\
&= \int_{t_i}^{t_i+\Delta t} \frac{\sqrt{V(\phi_0)}}{\sqrt{3}} \quad \mathrm{d}t = -\frac{2\dot{\phi}_0}{V'(\phi_0)} \frac{\sqrt{V(\phi_0)}}{\sqrt{3}} \\
\Delta N &\simeq \frac{2\sqrt{3(H(\phi_0))^2 - V(\phi_0)}}{V'(\phi_0)} \frac{\sqrt{V(\phi_0)}}{\sqrt{3}}.
\end{aligned}$$

[12] Here we interpret ϕ as taking generally different values during the time between the equivalent start and end values.

Figure 8

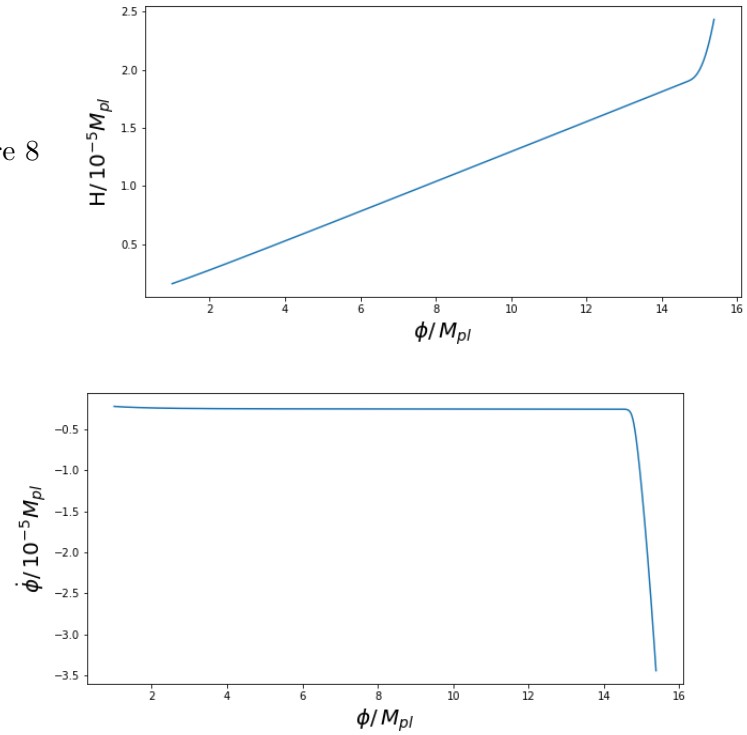

Figure 12: Example solutions to the HJ equation (11) generated by the numerical scheme we have developed - see *Numerical HJ examples.ipynb* in `https://github.com/jacb1729/DynamicsofCosmoinflation2021`. These plots correspond to $N = 56$ e-folds, with earliest state $H_b = 2.4 \times 10^{-5}, \phi_b = 15$ (all to 2sf). System parameters were $m = 2, V_0 = 0.05 \times 10^{-10}$. Solutions evolve from left to right forwards in time.

Remark 4. All solutions (including extended solutions) should grow exponentially in ϕ in the large ϕ limit in the $\phi - \dot{\phi}$ plane as well as the $\phi - H$ plane, using kinetic dominance for extended type A solutions and (28) for type B solutions, *except the separatrix*, so all type A or B trajectories for monomial potentials can be extended backwards to begin at the $\varepsilon = 1$ boundary.

5.6 Some results of simulations

Our first results come from *Numerical HJ examples.ipynb*, found in my `repository` for this project.

Once we have a **numerical solution**, an ordered list of ϕ values and a corresponding list of H values, we can convert the result to a trajectory in the $\phi - \dot{\phi}$ plane. For $\dot{\phi} < 0$, we note

$$\dot{\phi} = -2H' = -\sqrt{6H^2 - 2V}. \tag{33}$$

The same, but with opposite sign, is true for $\dot{\phi} > 0$. The result is shown in figure 12.

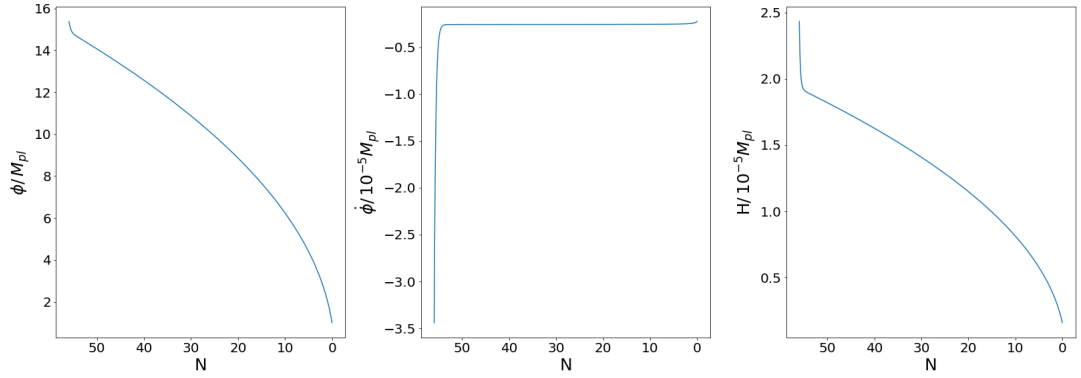

Figure 13: Example solutions to the HJ equation (11) generated by the numerical scheme we have developed (as in the previous figure). Plots correspond to the same solution as generated in the previous figure. Solutions evolve from left to right forwards in time.

To each numerical solution, the scheme associates a list of N values, which can be used to create a complementary plot like figure 13.

The reader is encourage to experiment with the software in *Numerical HJ examples.ipynb* to test its predictive range for themselves. An initial test one might conduct would be to consider the case $m = 0, V_0 = 0$ which should be an exponential solution. To get good results for this case, the user should also select `suppress=True`, `epsilonstop=False`, and select a larger initial step size for the sake of speed, for instance `dphi0=0.001`.

6 Phase portrait in the $\phi - \dot{\phi}$ plane

Our concluding result will be to generate a phase portrait which displays a signature of a separatrix solution and compare this to data. We can do this running the numerical scheme that we have just generated multiple times, but this code is far from optimised for convenient phase portrait generation. For now, we employ a dirty trick which motivates a promising line of inquiry.
Figures for this section appear at the end of the document.

Figure 14 (left) is generated using the numerical scheme we have developed. The curve along which trajectories collect is the separatrix. However, the user needs to make manual corrections to the maximum number of steps for a trajectory so that this runs in a feasible amount of time. We hope to capture the separatrix in the same detail via a faster, more convenient method. To do this, we re-introduce the dual dynamical system described by (29) as a 2-equation system of ODEs

$$\dot{\phi} = \varphi, \tag{34}$$

$$\dot{\varphi} = -\sqrt{3}\varphi\sqrt{\frac{1}{2}\varphi^2 + V(\phi)} + V'(\phi). \tag{35}$$

By defining this vector field appropriately, we can use streamline generator `matplotlib.pyplot.streamplot` to capture the dynamics with surprising accuracy (see 14). The function uses an adaptive RK2 integrator to predict the next step of a dynamics on a mesh in in phase space and hence produce integral curves of the vector field given; we shall give `steamplot` the field above. One weakness is that `streamplot` habitually creates unexpected blank patches because the function compromises where many solution curves would collect into the separatrix so to keep the density of lines fairly close to the specification. Luckily, such absences do not omit interesting information; the function appears to work well everywhere but one side of the separatrix's neighbourhood, so by process of elimination it highlights the separatrix curve well and is thus a promising candidate to describe phase portraits. The reason we proceed confidently is that the HJ scheme and `streamplot` agree as far as experimentation tells on the phase portrait, so we will use `streamplot` as a feasible alternative.

6.1 Restricting the phase space with Planck data

As in the $\phi - H$ plane perspective, we can write key observables in terms of ϕ and $\dot{\phi}$. Using (10) and (11), we write ε as

$$\varepsilon = \frac{3\dot{\phi}^2}{\dot{\phi}^2 + 2V}. \tag{36}$$

This is the formulation of ε that we used to approximate ΔN in the previous section. By (18),

$$r = \frac{48\dot{\phi}^2}{\dot{\phi}^2 + 2V}. \tag{37}$$

Bearing (25), (27) in mind, we are also able to write η and n_s in ϕ and $\dot{\phi}$, though the computation is tedious so is confirmed in *$r - n_s$calc2.mw*, *$r - n_s$calc.pdf*.

$$\eta = 6\frac{\dot{\phi}^2}{\dot{\phi}^2 + 2V} + 12\frac{\ddot{\phi}}{\dot{\phi}\sqrt{6\dot{\phi}^2 + 12V}}, \tag{38}$$

$$n_s = \frac{-7\dot{\phi}^3 - 2V'\sqrt{6\dot{\phi}^2 + 12V} - 11\dot{\phi}V}{\dot{\phi}\left(V - \dot{\phi}^2\right)}. \tag{39}$$

Additionally, we may invert the relations. Rearranging (37) and taking the negative solution (for values of r much smaller than 48),

$$\dot{\phi} = -\frac{\sqrt{2Vr(48 - r)}}{48 - r}.$$

Substituting this into (38), requiring $\phi > 0$, and requiring small r (in *Inverting r and n_s for phi and phidot.mw* I assert $r < 0.2$) gives only possible formulae for ϕ for magnitudes

$(n_s, r) \in (0, 0.2) \times (0.95, 1)$.

$$\phi = 8\frac{\sqrt{2}\,(48 - r)\,m}{\sqrt{r}\,(176 + r + 16 - n_s r)}. \tag{40}$$

Without asserting $\phi > 0$, we would have that $\pm\phi$ solves these relations if ϕ does. Also ignoring the condition $\dot{\phi} < 0$ would give the same two solutions for ϕ, but for our choice of $\phi > 0$ we may assume, based on phase portraits, that the positive $\dot{\phi}$ solution to the relations we have just derived does not correspond to the presence of a separatrix. Note finally that $\dot{\phi}$ is uniquely determined by ϕ by these relations:

$$\dot{\phi} = -V_0^{\frac{1}{2}}\sqrt{\frac{2r\left(8\frac{\sqrt{2}(48-r)m}{\sqrt{r}(176+r+16n_s-n_s r)}\right)^m}{48 - r}}.$$

In this model, given restrictions on r and n_s, r is the dominant parameter.

Thus, we can plot the data [3] (from which we derive figure 4) in the $\phi - \dot{\phi}$ plane. Consistently, the data maps to a region along the attractor (figure 15), with distributions typified by figure 16.

7 Conclusion

During this project, I have designed and written a numerical scheme for numerically solving the Hamilton-Jacobi equation (11) in the case of monomial potentials $V = V_0\phi^m$ for $V_0, m > 0$ (as a toy case), though strategy of the scheme should be effective for a much broader class of potentials when the exact code is generalised. Exacerbated by the existence of separatrices (often called attractors) of (11) for sensible potentials V, fixed step-size schemes prove insufficient. The work presented recently in [5] provides good tools to consider the global dynamics, and for the purposes of developing good numerical schemes usefully explains the extent of necessary complications to overcome.

Insights

- I have derived a formula for which gives the point in the phase space implied by given (sensible) values of observables r and n_s introduced in section 4.
- We have argued for the generic shape of the phase portrait based on experimentation, existence of separatrices and the kinetic dominance behaviour mentioned at the end of section 5.4.
- There is reason to believe that n_s and r restrictions [3] correspond to curves lying very close to the separatrix. Thus, in the absence of globally specified solutions, separatrix solutions should pose good representations of evolutions. Potentially, this

could introduce a swift method of predicting the location of separatrices.

- One justification for using SR models is the expectation that they correspond to 'attractors'. We have a method of generating correction to this idea.

Areas of interest

- One last noteworthy result is the promise that a general adaptive scheme could be of use too, based on the accuracy with which `matplotlib.pyplot.streamplot` appears to describe the phase portrait relative to the scheme we have developed. This inbuilt function employs an adaptive RK2 integrator, as opposed to the bespoke RK4 scheme we have developed, and is much faster, so one simple way to make the scheme we have developed more efficient could be inspired by the source code for `streamplot`.
- The code in *Numerical HJ examples.ipynb* is still only suitable for monomial potentials, so a possible next step would be generalising this code; in particular, we should extend the scheme to work for potentials which define exactly solved models against which the scheme can be tested. On the other hand, it would be easier to generalise a `streamplot`-based scheme because it is easier to generalise the vector field function to an effectively unrestricted class of potentials.
- A later prospect would be incorporate good separatrix bounds into the algorithm - currently, we assume that the separatrix is arbitrarily close to the $\varepsilon = 0$ curve when calculating step-sizes, which we know to be false.
- Given boundless time, I would first try to develop methods to calculate separatrices. Calculations which I still need to check give the large ϕ asymptotic solutions for monomial potentials with, and Álvarez et al[5] have noted some more general tools for the study of separatrix asymptotes, so I would hope for tools to place good restrictions on solutions given asymptotic information.
- Another useful move would be to quantify the stepwise error that this or a descendent scheme produces in solutions - all we currently know is based on order estimates given by our use of RK4 integrator.
- I would like to investigate dependence of r on the wave-vector k of perturbations. For monomial potentials, it appears that smaller r values correspond roughly to earlier points of inflation, which would suggest that inflation coincided with an increase in the energy scale of the universe until sufficient energy was reached to cause the medium (be it an inflaton field or otherwise) to transform. The dependence in this model would not have been picked up due to wave-vectors corresponding to too narrow a range of times during inflation, but we should consider the map of r and n_s data into the $\phi - \dot{\phi}$ plane for other potentials in evaluating this.

Appendix 1 - Derivations

Derivation of η in HJ inflation

We derive equation (22) here.

$$\eta = \frac{1}{H}\frac{\mathrm{d}}{\mathrm{d}t}\log\varepsilon = \frac{\dot\phi}{H}\frac{\mathrm{d}}{\mathrm{d}\phi}\log\varepsilon = \frac{\dot\phi}{H}\frac{\frac{\mathrm{d}}{\mathrm{d}\phi}\left(\frac{H'}{H}\right)^2}{\left(\frac{H'}{H}\right)^2}.$$

Now we split the calculation:

$$\frac{\dot\phi}{H}\left(\frac{H'}{H}\right)^{-2} = \frac{H}{H'^2}\dot\phi,$$

$$\frac{\mathrm{d}}{\mathrm{d}\phi}\left(\frac{H'}{H}\right)^2 = 2\frac{H'}{H}\left(\frac{H''}{H} - \frac{H'^2}{H^2}\right)$$

Therefore, using $\dot\phi = -2H'$,

$$\eta = 2\frac{\dot\phi}{H'}\left(\frac{H''}{H} - \frac{H'^2}{H^2}\right) = 2\varepsilon - 4\frac{H''}{H}.$$

References

[1] Tasi lectures on inflation: 1, . URL `https://www.youtube.com/channel/UCHJpr2MfesuQN6EMObzUv4A`.

[2] Tasi lectures on inflation: 2, . URL `https://www.youtube.com/watch?v=Sad6kAq4JlU`.

[3] Baseline LCDM chains with baseline likelihoods, 2018.

[4] Y. Akrami, F. Arroja, M. Ashdown, J. Aumont, C. Baccigalupi, M. Ballardini, A. J. Banday, R. B. Barreiro, N. Bartolo, and et al. Planck 2018 results. 641:A10, Sep 2020. ISSN 1432-0746. doi: 10.1051/0004-6361/201833887. URL `http://dx.doi.org/10.1051/0004-6361/201833887`.

[5] Gabriel Álvarez, Luis Martínez Alonso, Elena Medina, and Juan Luis Vázquez. Separatrices in the hamilton–jacobi formalism of inflaton models. *Journal of Mathematical Physics*, 61(4):043501, 2020.

[6] Vladimir Igorevich Arnol'd. *Mathematical methods of classical mechanics*, volume 60. Springer Science & Business Media, 2013.

[7] Daniel Baumann. Tasi lectures on inflation, 2012.

[8] William E Boyce. *Elementary Differential Equations and Boundary Value Problems 8th Edition O.* John Wiley & Sons, 2007.

[9] Robert Brandenberger. Initial conditions for inflation—a short review. *International Journal of Modern Physics D*, 26(01):1740002, 2017.

[10] S Capozziello, R De Ritis, C Rubano, and P Scudellaro. Noether symmetries in cosmology. *La Rivista del Nuovo Cimento (1978-1999)*, 19(4):1–114, 1996.

[11] Bradley W. Carroll and Dale A. Ostlie. *An Introduction to Modern Astrophysics.* Pearson Education Limited, 2013.

[12] R De Ritis, G Marmo, G Platania, C Rubano, P Scudellaro, and C Stornaiolo. New approach to find exact solutions for cosmological models with a scalar field. *Physical Review D*, 42(4):1091, 1990.

[13] Scott Dodelson. *Modern cosmology.* Elsevier, 2003.

[14] Edwin Hubble. A relation between distance and radial velocity among extra-galactic nebulae. *Proceedings of the national academy of sciences*, 15(3):168–173, 1929.

[15] J. D. Hunter. Matplotlib: A 2d graphics environment. *Computing in Science & Engineering*, 9(3):90–95, 2007. doi: 10.1109/MCSE.2007.55.

[16] Andrew Liddle. *An Introduction to Modern Cosmology.* John Wiley and Sons, 2015.

[17] Andrew R. Liddle and David H. Lyth. *Cosmological Inflation and Large-Scale Structure.* Cambridge University Press, 2000. doi: 10.1017/CBO9781139175180.

[18] Chung-Pei Ma and Edmund Bertschinger. Cosmological perturbation theory in the synchronous and conformal newtonian gauges. *arXiv preprint astro-ph/9506072*, 1995.

[19] Viatcheslav Mukhanov. *Physical foundations of Cosmology.* Cambridge university press, 2005.

[20] Viatcheslav F Mukhanov, Hume A Feldman, and Robert Hans Brandenberger. Theory of cosmological perturbations. *Physics reports*, 215(5-6):203–333, 1992.

[21] Saul Perlmutter, Goldhaber Aldering, Gerson Goldhaber, RA Knop, Peter Nugent, Patricia G Castro, Susana Deustua, Sebastien Fabbro, Ariel Goobar, Donald E Groom, et al. Measurements of ω and λ from 42 high-redshift supernovae. *The Astrophysical Journal*, 517(2):565, 1999.

[22] Grant N Remmen and Sean M Carroll. Attractor solutions in scalar-field cosmology. *Physical Review D*, 88(8):083518, 2013.

[23] Shinji Tsujikawa. Introductory review of cosmic inflation, 2003.

[24] Steven Weinberg. *Gravitation and cosmology: principles and applications of the general theory of relativity.* 1972.

Acknowledgements

To my parents, for their unwavering example and encouragement towards science and engineering. I am glad to have only escaped at the 11^{th} hour to end up in mathematics.

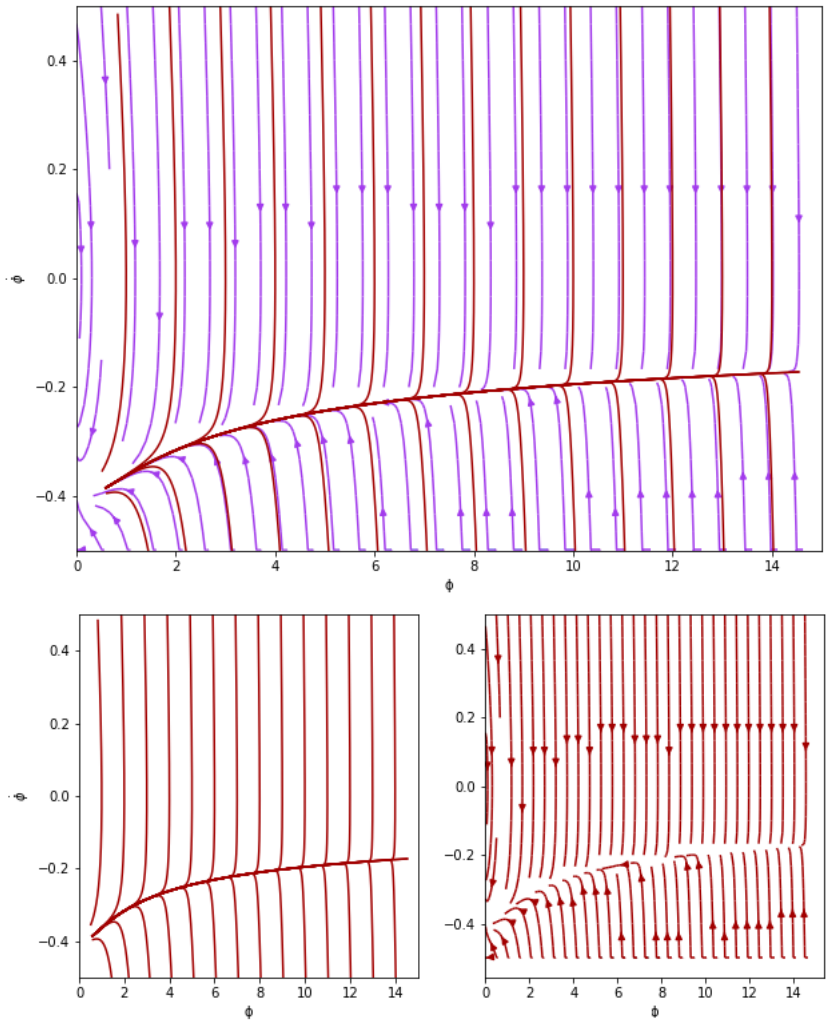

Figure 14: Left: Phase portrait generated by running several iterations of the numerical integration scheme developed in this project. Running forwards in time, points move along the integral curves illustrated towards the separatrix, then evolve left. Right: Phase portrait generated using the `matplotlib.pyplot.streamplot` from the system of ODEs (34), (35). Points evolve forwards in time as illustrated by the arrows, but the separatrix is not explicitly shown due to necessary line-density restrictions inbuilt into `streamplot`. Top: Phase portraits generated by both methods superposed. Crucially, the separatrix location and so-called kinetic dominance regions agree seamlessly.

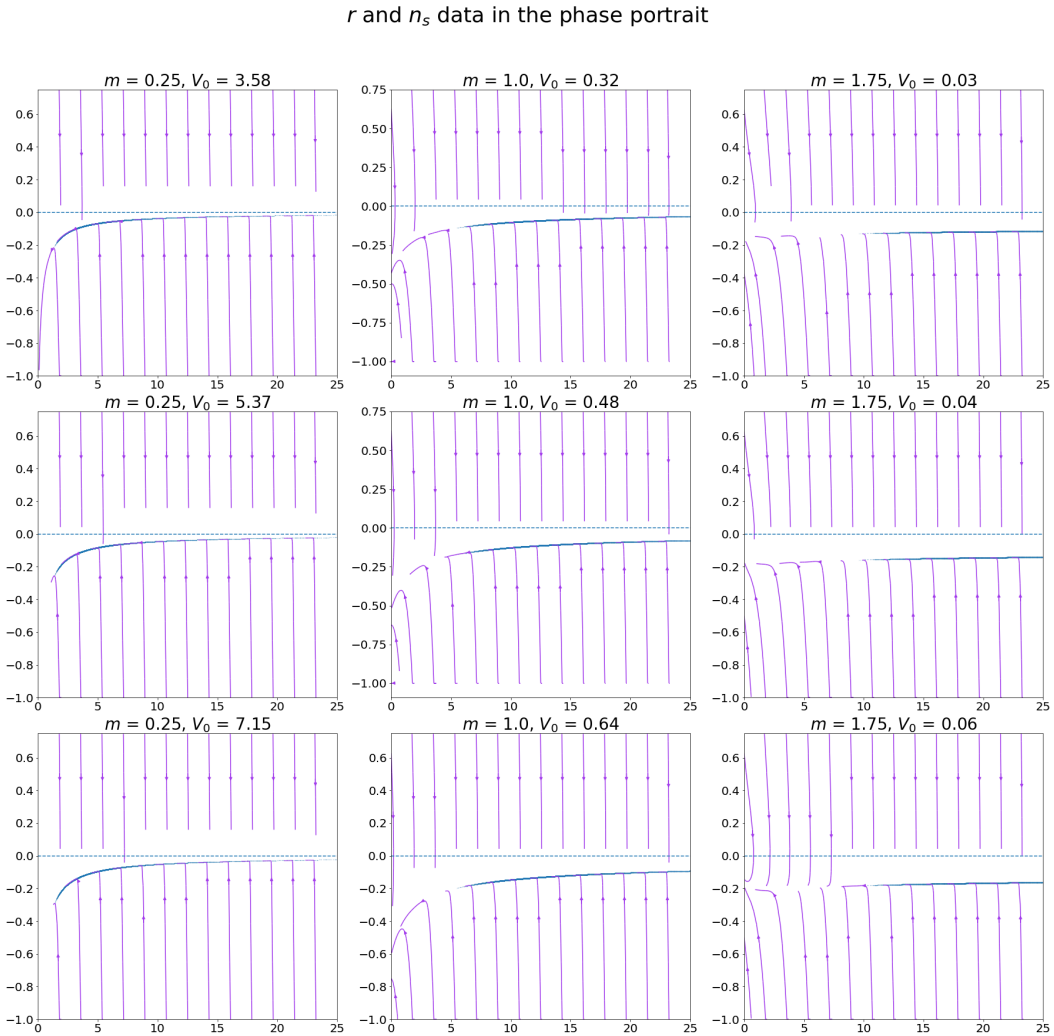

Figure 15: Having determined equations to calculate the phase space values corresponding to given data points on observables r, n_s[3] (verification in *Inverting r and n_s for phi and phidot.mw*, see repository), we map the data onto phase portraits of the dynamics first posed in section 3, approximated using `matplotlib.pyplot.streamplot`. We find enticing evidence in favour of initial conditions at time corresponding to $N \gtrsim 60$ being close to the separatrix.

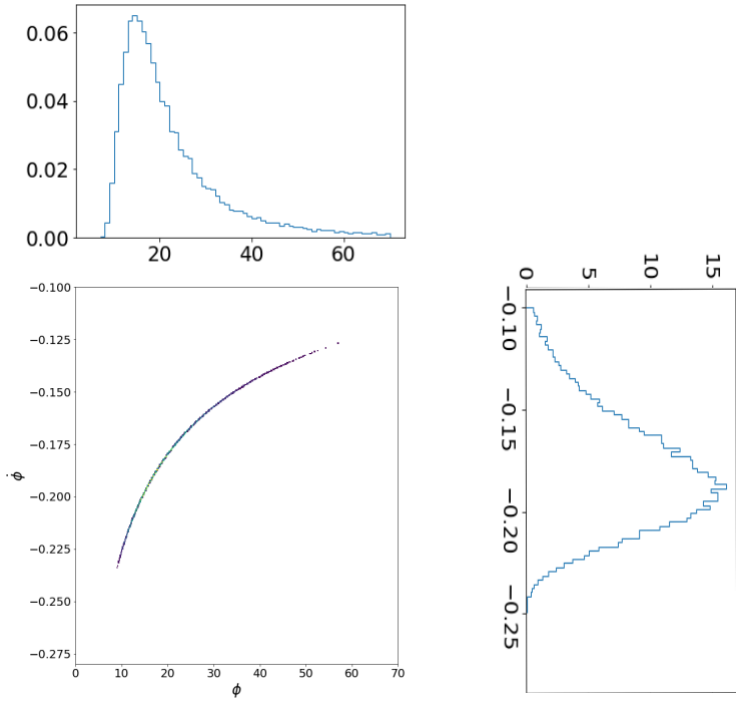

Figure 16: Data [3] which generates figure 4 is mapped under the relations we have determined (for a choice of parameters) to give a distribution of data points; their densities in the $\phi - \dot{\phi}$ plane are illustrated in the central figure, which is generated as a histogram (see *phasespace limits.ipynb*). Lighter colours (except the white background) indicate higher densities of points mapped in the locality of that point. The (marginal) density distribution of ϕ and $\dot{\phi}$ are also shown on separate sub-plots to form a variant of the triangle plot.